Eur. Phys. J. A (2020) 56:26
https://doi.org/10.1140/epja/s10050-020-00032-z

THE EUROPEAN PHYSICAL JOURNAL A

Special Article - New Tools and Techniques

Measurement of neutron and proton analyzing powers on C, CH, CH_2 and Cu targets in the momentum region 3–4.2 GeV/c

S. N. Basilev[1], Yu. P. Bushuev[1], O. P. Gavrishchuk[1], V. V. Glagolev[1], D. A. Kirillov[1], N. V. Kostayeva[1], A. D. Kovalenko[1], K. S. Legostaeva[1], A. N. Livanov[1], I. A. Philippov[1], N. M. Piskunov[1], A. A. Povtoreiko[1], P. A. Rukoyatkin[1], R. A. Shindin[1], A. V. Shipunov[1], A. V. Shutov[1], I. M. Sitnik[1], V. M. Slepnev[1], I. V. Slepnev[1], A. V. Terletskiy[1], K. Hamilton[2], R. Montgomery[2], J. R. M. Annand[2], D. Marchand[3], Y. Wang[3], E. Tomasi-Gustafsson[4,a], C. F. Perdrisat[5], V. Punjabi[6], G. Martinska[7], J. Urban[7], J. Mušinsky[8]

[1] Joint Institute for Nuclear Research, 141980 Dubna, Russia
[2] University of Glasgow, Glasgow G12 8QQ, Scotland, UK
[3] IPN Orsay, Université Paris-Saclay, 91406 Orsay, France
[4] IRFU, CEA, Université Paris-Saclay, 91191 Gif-sur-Yvette, France
[5] The College of William and Mary, Williamsburg, VA 23187, USA
[6] Norfolk State University, Norfolk, VA 23504, USA
[7] University of P.J. Safarik, Jesenna 5, 04154 Košice, Slovak Republic
[8] Institute of Experimental Physics, Watsonova 47, 04001 Košice, Slovak Republic

Received: 16 August 2019 / Accepted: 26 November 2019 / Published online: 28 January 2020
© Società Italiana di Fisica (SIF) and Springer-Verlag GmbH Germany, part of Springer Nature 2020
Communicated by P. Rossi

Abstract The analyzing powers for proton elastic scattering ($\boldsymbol{p}A \to pX$) and neutron charge exchange ($\boldsymbol{n}A \to pX$) reactions on nuclei have been measured on C, CH, CH_2 and Cu targets at incident neutron momenta 3.0–4.2 GeV/c by detecting one charged particle in forward direction. The polarized neutron measurements are the first of their kind. The experiment was performed using the Nuclotron accelerator in JINR Dubna, where polarized neutrons and protons were obtained from break-up of a polarized deuteron beam which has a maximum momentum of 13 GeV/c. The polarimeter ALPOM2 was used to obtain the analyzing power dependence on the transverse momentum of the final-state nucleon. These data have been used to estimate the figure of merit of a proposed experiment at Jefferson Laboratory to measure the recoiling neutron polarization in the quasi-elastic $^2H(\boldsymbol{e}, e'\boldsymbol{n})$ reaction, which yields information on the charge and magnetic elastic form factors of the neutron.

1 Introduction

Polarimetry of nucleons in the GeV region requires the measurement of the azimuthal distribution resulting from a secondary scattering of the polarized nucleon in a suitable analyzing material. C or CH_2 are often used as the analyzers in proton polarimeters. Analyzing power measurements were made at Saclay [1] (and the references therein) and Dubna [2], using thick analyzers, and as part of a program of study of elastic and quasi-elastic $\boldsymbol{d}p$ reactions [3] up to incident momenta of several GeV/c. New measurements at Dubna will extend the incident momenta up to 7.5 GeV/c [4].

Up to now neutron polarimetry has generally been based on free elastic np scattering or elastic-like np scattering from nuclei. The kinematic reconstruction of the scattering process is highly desirable to select the range of polar scattering angles where the analyzing power is relatively large. This may be achieved by using an active, position-sensitive analyzer to detect the recoiling proton and thus localise the interaction position of the incident neutron. Alternatively charge-exchange neutron scattering may be used, where the trajectory of the energetic, forward-angle proton can be tracked.

In comparison to proton scattering, the analyzing power A_y for polarized neutron scattering at GeV energies is poorly known. Analyzing powers for $n + p \to n + p$ and $n + p \to p + n$ scattering exist only for thin ^1H or ^2H targets. Free np scattering is in principle the best analyzer of neutron polarization, but the use of a hydrogen analyzer is challenging technically and up to now scattering from C, CH or CH_2 has most commonly been used. However, A_y for elastic-like scattering from nuclei is unknown in the few-GeV energy range and will be lower than for the free-scattering case.

[a] e-mail: egle.tomasi@cea.fr

Polarized deuteron beams up to 13 GeV/c momentum, producing polarized neutron and protons after break-up, are presently available only at the Nuclotron accelerator in Dubna. An important upgrade of the accelerator complex has been recently undertaken [5], as a first step of the future NICA collider [6]. This resulted in a new program by the ALPOM2 collaboration, with the aim to measure analyzing powers up to the largest available momenta [4]. The experimental program and the first results with polarized neutrons are reported here.

These data are particularly important for pursuing the nucleon electromagnetic form factor measurements at JLab.

1.1 Proton form factor measurements

The electromagnetic form factors (EMFFs) of elastic electron–nucleon (eN) scattering are representative of the charge and the magnetic currents of the nucleons (for recent reviews on electromagnetic form factors see Refs. [7,8]).

Early determinations of the EMFF used Rosenbluth separation of differential cross section measurements [7], but as electron accelerator technology has developed to produce high-current, high-polarization, continuous-wave electron beams, the measurement of polarized observables has become the method of choice. Polarization observables are especially useful in separating a small amplitude from an otherwise dominant one and are believed to be relatively insensitive to radiative correction effects.

The use of polarization was first proposed in Refs. [9,10] by the Kharkov school as an alternate method to Rosenbluth separation to determine the nucleon EMFF from polarized elastic electron-proton ($\boldsymbol{e}p$) and electron-neutron ($\boldsymbol{e}n$) scattering (where the neutrons are bound in a deuteron or ^3He target). The ratio of the longitudinal to transverse recoil-nucleon polarization in elastic eN scattering, with longitudinally polarized electrons, is proportional to the ratio of electric to magnetic form factors, whereas the unpolarized cross section depends on the squares of form factors. These types of double-polarization experiments, denoted, in the following, *recoil polarization experiments* , require the measurement of the polarization of the recoiling nucleon in elastic eN scattering. Experiments of this type started in the 1990s (see below) when high-intensity, highly-polarized, high-duty-cycle electron beams became available.

Subsequently, the range of the squared four-momentum transfer, Q^2, has been extended at Jefferson Lab (JLab), using a polarized electron beam of energy up to 5.7 GeV to measure the four form factors of elastic eN scattering (electric and magnetic, for proton and neutron, G_E^p, G_M^p, G_E^n, G_M^n). Proton data have produced unexpected and intriguing results. Contrary to the generally accepted scaling relation that the electric to magnetic form factor ratio $\mu_p G_E^p/G_M^p \sim 1$ ($\mu_p = 2.79\mu_N$ is the proton anomalous magnetic moment)

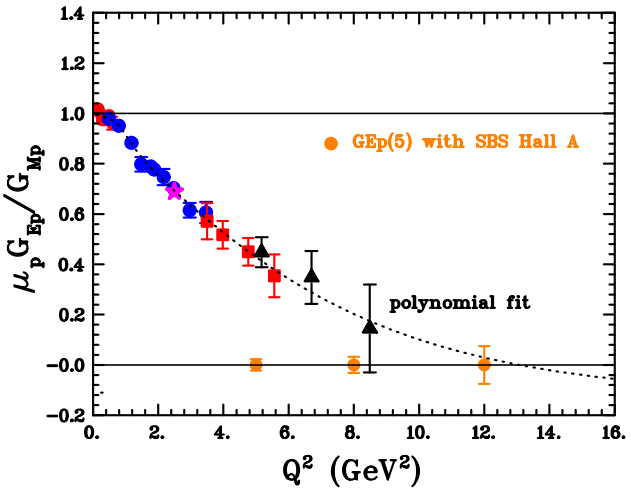

Fig. 1 Projections of experimental uncertainties for future JLab experiment E12-07-109 [18] (filled orange circles). Also shown for comparison are previous JLab G_E^p/G_M^p data for GEp(1), GEp(2), GEp(3), and GEp2γ [11–17]. The dotted line is a polynomial fit

the recoil polarization data show an approximately linear decrease of this ratio, clearly indicating that the electric and magnetic form factors have different dependences on Q^2, and therefore that the radial distributions of charge and magnetization are not the same. This was an unexpected result and the various papers publishing these results [11–17] have been cited more than 2000 times.

JLab has recently undergone an energy upgrade, and is producing polarized beams of energy up to 11 GeV. Extending the Q^2 range of $\mu_p G_E^p/G_M^p$ measurements should determine if the ratio does cross zero, as suggested by the existing data, while for $\mu_n G_E^n/G_M^n$ a completely virgin territory will be explored. With an increase in Q^2 the momentum of the recoiling nucleon also increases. Approval of the most recently published G_E^p/G_M^p experiment [16] relied heavily on measurements previously made at Dubna [2], which showed that the proton analyzing power at high momentum is sufficiently large to obtain a good precision for the EMFF ratio. Therefore the extension of the analyzing power data base to higher nucleon momenta is urgently needed, both for protons and, more critically, for neutrons where multi-GeV/c data are extremely limited. The status and the planned experiments for nucleon EMFF are briefly reviewed here.

Experiment E12-07-109 [18] will measure the proton form factor ratio up to $Q^2 = 12$ (GeV/c)^2, and a projection of the achievable precision is displayed in Fig. 1. To achieve this, a high luminosity of 10^{39} cm^{-2}s^{-1} and a large acceptance detector are necessary. The electron arm will consist in a Pb-Glass calorimeter, while the proton recoil polarimeter will be part of the Super Bigbite Spectrometer (SBS) spectrometer. The SBS is equipped with a large-aperture dipole magnet of 1.7 Tm integrated field strength, two 60 cm CH_2 ana-

lyzer blocks, ten planes of GEM chambers for proton tracking before and after the analyzers and a hadron calorimeter to select energetic protons in the experimental trigger.

1.2 Neutron form factor measurements

Measurements of neutron elastic form factors generally use quasi-elastic $(e, e'n)$ scattering from the neutron embedded in a ^2H or ^3He target, where the scattered electron and recoiling neutron are detected in coincidence. Quasi-elastic scattering is separated from inelastic processes on the basis of the measured electron momentum and the angular correlation of the e' and n.

The first recoil polarization measurement of G_E^n/G_M^n was made at Bates Laboratory [23], but the achieved precision was limited, mainly due to lack of a Continuous-Wave (CW) electron beam. Following on from this, a polarized CW 855 MeV electron beam became available at the MAMI accelerator in Mainz and a series of recoil polarization measurements were made with an unpolarized, liquid D_2 target [26,28], in parallel with measurements using a polarized ^3He target. Subsequent measurements at MAMI were made in the A1 spectrometer hall [24] using a high resolution magnetic spectrometer to detect the e' and a more compact plastic-scintillator, neutron polarimeter. At MAMI, recoil polarization measurements extended to $Q^2 = 0.8$ (GeV/c)^2, where Q^2 is limited by the maximum electron beam energy (currently 1.6 GeV). In JLab Hall-C, using the 6 GeV CEBAF accelerator, recoil polarization measurements extended up to $Q^2 = 1.45$ (GeV/c)^2 [31,32]. Using a polarized ^3He target in Hall-A [33], a maximum value of $Q^2 = 3.4$ (GeV/c)^2 was achieved.

Two new recoil polarization measurements of G_E^n/G_M^n have been proposed to run at the upgraded 11 GeV CEBAF accelerator. The first follows on from the previous Hall-C experiments [19], while the second in Hall-A [20] proposes a polarimeter to measure charge-exchange neutron scattering from Cu. The present charge-exchange results, used to estimate (see below) the figure of merit of the polarimeter and hence the obtainable experimental precision, played a crucial role in the approval of this new polarimetry technique for E12-17-004.

Selected data are shown in Fig. 2, together with the projected future results (cyan symbols). The lines are the predictions from a polynomial fit and from a Dyson–Schwinger approach from [30].

1.3 Polarimetry in the GeV region

The information on polarized nucleon scattering for incident momenta $p_{lab} \geq 1.5$ GeV/c (Fig. 3) comes from a number of sources. Measurements of the asymmetries of the $d(\boldsymbol{p}, p')n$ and $d(\boldsymbol{p}, n)p$ processes have been performed in the 1970s up to an incident momentum of 11 GeV/c [34,35]. The $d(\boldsymbol{p}, p')n$ data are consistent with elastic $\boldsymbol{p}+p \rightarrow p+p$ measurements [36] so that these experiments are equivalent to free polarized pp and pn scattering. Inclusive measurements of $\boldsymbol{p}+CH_2 \rightarrow p+X$ [2], and $\boldsymbol{p}+C \rightarrow p+X$ have been obtained for the calibration of proton polarimeters used at ANL, JINR Dubna and JLab [1,37].

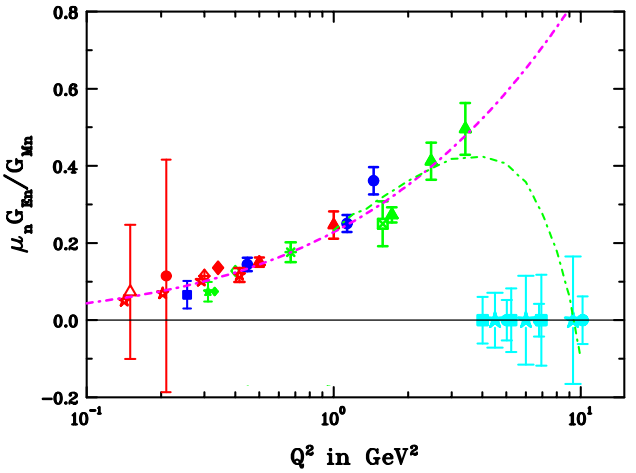

Fig. 2 The future data points proposed for recoil polarization G_E^n/G_M^n experiments at JLab [19] (filled cyan squares), [20] (filled cyan stars), and the JLab polarized ^3He experiment (filled cyan circles) [21]. Also shown are the data from Becker (filled green diamonds) [22], Eden (filled blue squares) [23], Glazier (red diamonds with internal +) [24], Golak (empty green diamonds) [25], Herberg (empty red triangles) [26], Meyerhof (filled green stars) [27], Ostrick (filled red diamonds) [28], and Passchier (filled red circles) [29]. The green dashed line is the predictions from a Dyson–Schwinger approach [30], the pink dotted line is a polynomial fit

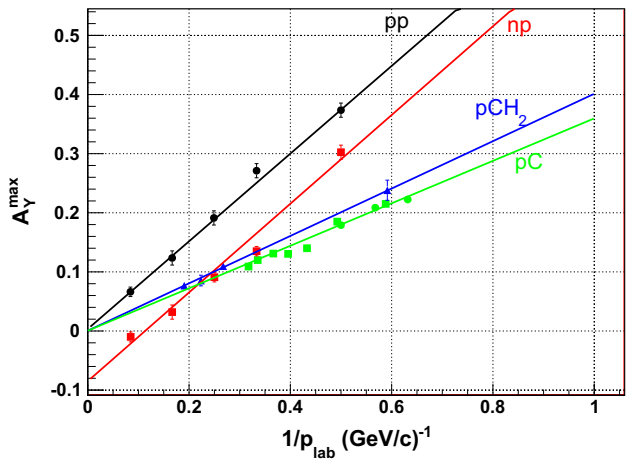

Fig. 3 The dependence of the maximum of A_Y on the inverse of p_{lab}, the momentum of the proton entering the polarimeter in the laboratory system. Black circles: ANL $d(\boldsymbol{p}, p')n$ data [34,35]; black line: linear fit. Red squares: ANL $d(\boldsymbol{p}, n)p$ data [1,37]; red line: linear fit. Blue triangles [2]: $\boldsymbol{p} + CH_2 \rightarrow charged + X$; blue line: linear fit [2]. Green squares [1] and circles [37]: $\boldsymbol{p} + C \rightarrow charged + X$; green line: linear fit [2]

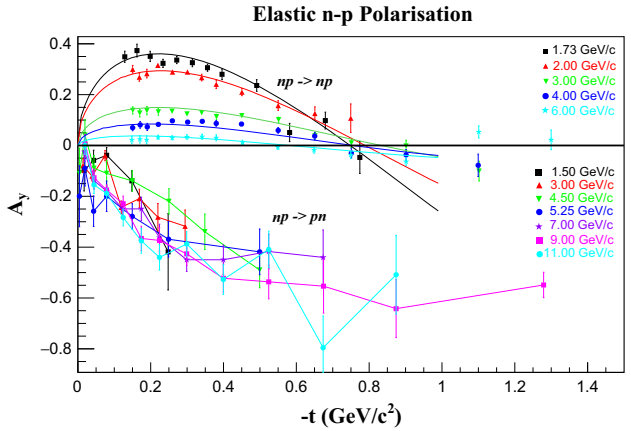

Fig. 4 Top: t-dependence of the polarisation of np scattering for different values of p_{lab} [34,35]. The smooth dotted lines show the fit of Ref. [38] to the np data. Bottom: the t-dependence of charge-exchange $n\boldsymbol{p}$ scattering, for different values of p_{lab} [39,40]. The color coding relates the data to momentum labels

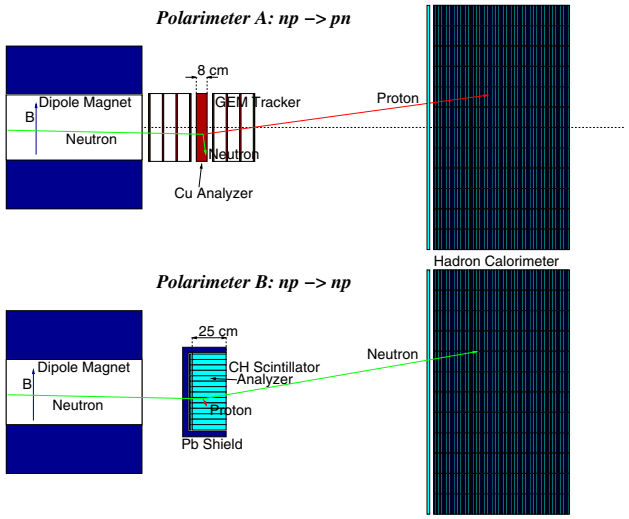

Fig. 5 Neutron polarimeter configurations considered in the simulations- Polarimeter A for charge-exchange reactions (top); Polarimeter B for elastic scattering (bottom)

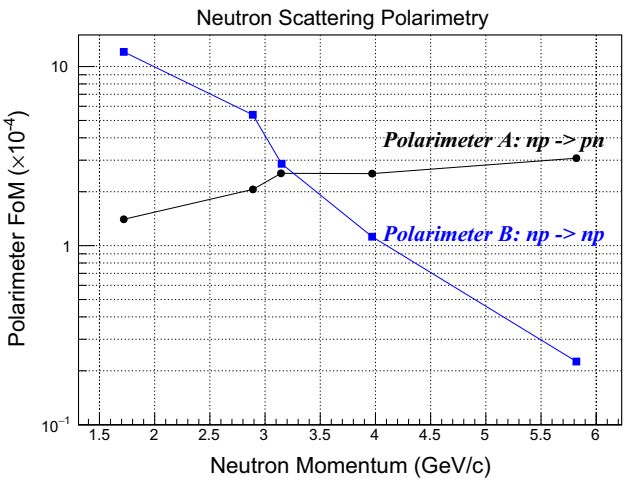

Fig. 6 Neutron polarimeter figure of merit as a function of incident neutron momentum for the two polarimeter configurations of Fig. 5. Blue squares: standard np scattering from CH scintillator (Polarimeter **b**), black circles: charge-exchange np scattering from Cu (Polarimeter **a**)

The data displayed in Fig. 3 show an approximately linear dependence of the maximum value of the angle dependent analyzing power, A_y^{max}, on $1/p_{lab}$, but there is a significant negative offset of the pn data with respect to pp. There is a factor of 2 reduction in the analyzing power of $\boldsymbol{p}+^{12}C$ with respect to free pp scattering, but to our knowledge there are no data on polarized np scattering from nuclei in the multi-GeV energy domain.

Measurements of the asymmetries of polarized charge-exchange $n+\boldsymbol{p}\rightarrow p+X$ scattering, displayed in Fig. 4 up to 11 GeV/c, have also been made at ANL in the 1970s [39, 40]. While the np (equivalent to pn) polarization is strongly dependent on the incident nucleon momentum p_{lab}, charge-exchange np displays no apparent (given the spread in the data) strong dependence of A_y on p_{lab}.

The performance of a polarimeter is usually expressed in terms of the figure of merit (FOM), defined as

$$F^2(p)=\int \epsilon(p,\theta')\,A_y^2(p,\theta')d\theta' \qquad (1)$$

where p is the incident momentum, θ' is the nucleon scattering angle, ϵ is the ratio of number of useful over incident events and A_y is the effective analyzing power of the polarimeter. FOM estimates have been calculated over a range of beam momenta for two polarimeter configurations (Fig. 5) employing either charge-exchange or elastic np scattering and are shown in Fig. 6.

Elastic-like pp scattering from nuclei is observed to have a factor-2 reduction in A_y, compared to the free elastic pp. For np, the same reduction factor is consistent with the polarimeter analyzing power obtained in a previous JLab measurement of G_E^n/G_M^n [31,32] at 1.45 GeV/c and is assumed for nC scattering. The value of A_y for free elastic np scattering has been calculated from a fit to the pn data [38]. For charge-exchange np scattering from Cu, A_y was taken from a preliminary analysis of the new data described in this paper. This analysis has given the dependence of A_y on $p_t=p_{lab}\sin\theta_{np}$ at an incident momentum of 3.75 GeV/c. A_y is dependent on p_t, but has been assumed independent of p_{lab}, in a manner consistent with the free charge-exchange np data.

Polarimeter efficiencies have been calculated using Geant-4-based Monte Carlo (MC) simulations of different polarimeter configurations (Fig. 5) that record the differential detection efficiency as a function of scattering angle, after selection of energy and angle ranges in a manner analagous to a real experiment. Calculations have been made for two versions

of the polarimeter, compatible with possible experimental configurations at JLab.

1. The polarimeter uses a passive Cu analyzer with forward-angle, charge-exchange proton detection by GEM trackers and hadron calorimeter (A).
2. The polarimeter employs an active position-sensitive CH (plastic-scintillator) analyser with forward-angle neutron detection by the hadron calorimeter (B).

At neutron momenta above $\sim$ 3.5 GeV/c, the FOM of charge-exchange np starts to dominate standard np and by $\sim$ 6 GeV/c it is projected to be a factor $\sim$ 15 larger. These calculations suggest strongly that polarimetry by charge-exchange scattering is the technique which will allow recoil polarization G_E^n/G_M^n to approach $Q^2 \sim$ 10 (GeV/c)^2.

2 The ALPOM2 experiment

2.1 The beam production

ALPOM2 is placed at the beam line '1v' of the Nuclotron accelerator facility, at the Veksler Baldin Laboratory for High Energy Physics (VBLHEP) of the Joint Institute for Nuclear Research in Dubna. This beam line was used previously for several experiments using (polarized) neutron beams [41], such as the measurement of the $\Delta\sigma(n^{\uparrow}p^{\uparrow})$ total cross section difference [42].

The polarized deuteron source is provided by the Source of Polarized Ions (SPI), which is a JINR and INR RAS development of the CIPOS source [43] formerly employed at the Indiana University Cyclotron Facility. SPI is an atomic beam polarized ion source with a plasma (H,D) charge-exchange ionizer and a storage cell in the ionization region The ions are preaccelerated to 100–150 keV in the LU-20 injector, and then accelerated by the Nuclotron [44].

The SPI operates either in polarized or unpolarized mode, following the principle to polarize particles through adiabatic transitions between two hyperfine structure levels, as established by Abragam [45].

The deuteron beam, extracted over a period of 5 s was incident on a 30(25) cm thick $C(CH_2)$ target where the deuteron was fragmented into a proton and a neutron. Experiments on polarization transfer from deuteron to proton in break-up reactions showed that the proton (and therefore the neutron) polarization is equal to the polarization of the primary deuteron beam and constant when the internal momenta of the nucleons inside the deuteron $q \leq 0.15$ GeV/c [46]. Thus, it is possible to produce polarized nucleons with momenta higher than half of the incident deuteron momentum. Deuterons with momentum of 12–13 GeV/c may produce protons of momentum up to 7.5 GeV/c with a polarization equal to that of the incident deuterons. However, the largest cross section is obtained by selecting secondary nucleons corresponding to $q = 0$. For the present measurement, the nucleon beam momentum was half the incident deuteron momentum

To produce a neutron beam, protons and deuterons were deflected out of beam by a dipole magnet. Neutron angles close to zero degrees were selected by a 6 m long collimator made of iron and brass located 13.4 m upstream from the ALPOM2 set-up. The collimators and shielding of the experimental area decreased the low energy tail of the neutron spectrum to about 1% of the peak value. By setting the primary deuteron beam intensity in the range 1–3$\times 10^8$ particles/spill, the average number of protons or neutrons incident on the polarimeter target was kept at the level of 4×10^4 per spill. The length of the spill depends on the primary beam intensity and in the present case was of the order of a few seconds. More details on the operation of the neutron beam line can be found in Refs. [41,47]. The polarization of the incident deuterons was oriented downwards, along the vertical axis, perpendicular to the beam momentum. The polarization of the produced nucleons (n or p) keeps the same direction.

2.2 Beam polarimetry

The accurate measurement of the secondary nucleon beam polarization is crucial to the extraction of the analyzing power in ALPOM2, as the beam-polarization uncertainty is the main source of the systematic error on the analyzing power. The polarized deuteron beam was tagged with its three polarization states, down (plus, '+', $P_z = +1$, $P_{zz} = +1$), up (minus, '−', $P_z = -1/3$, $P_{zz} = 0$), and unpolarized (zero, '0'), where the state is changed after each spill.

The beam polarimeter, denominated F3 as it is located at the focus F3 of the extracted beam line, is based on quasi-elastic pp scattering, where analyzing powers are known (within 10%) from previous measurements [48]. For example the analyzing power of the polarimeter at a momentum of 3.75 GeV/c is Ay = $0.20 + -0.02$. F3 has an ionization chamber (IC) as a beam intensity monitor for normalization, and four arms, forward and recoil, left and right. Each arm has three sets of scintillator counters at forward angle $\theta \simeq 8°$, 9°, and 10.5°, for momenta 4.2, 3.75 and 3 GeV/c, respectively, and a bigger scintillator at backward angle $\theta \simeq 60°$ for the recoil particle. The coincidence between forward and recoil arms (left and right) and the IC counts was collected, spill by spill, by the data acquisition system.

The nucleon beam polarization was constantly monitored and the stability of the beam was excellent. The fluctuations of the polarimeter asymmetry did not exceed 2%.

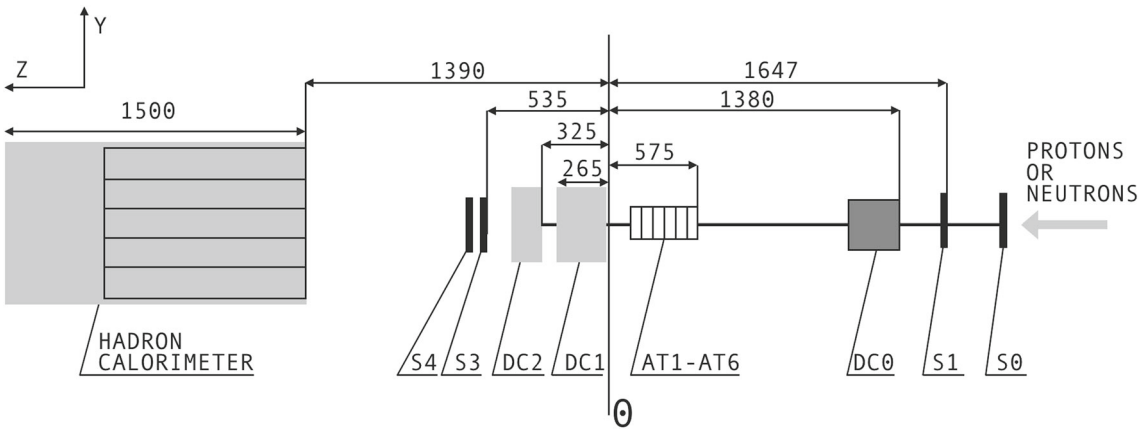

Fig. 7 Side view schematic of the ALPOM2 set-up positioned on the secondary proton/neutron beam line, including scintillation counters (S0, S1, S3, S4); drift chambers (DC0, DC1, DC2); hadron calorimeter. The analyzing targets were located between DC0 and DC1. Here a CH active target (AT1–AT6), is shown as an example. Dimensions are in mm. Θ indicates the origin of the z coordinate

2.3 The ALPOM2 setup

ALPOM2 represents an upgrade of the ALPOM polarimeter [2], which in turn is based on the POMME polarimeter employed at Saturne [49]. A schematic view of the ALPOM2 geometry is shown in Fig. 7, with the proton/neutron beam traveling along the z-axis, in the longitudinal direction.

The main components consisted of:

- fast plastic-scintillator counters (S0, S1, S3, S4 and optionally AT1-AT6) for triggering purposes;
- drift chambers (DC0, DC1, DC2) for charged particle tracking;
- a segmented hadron calorimeter for energy and position measurements of the outgoing particles;
- the polarimeter analyzer (C, CH, CH_2, Cu), where Fig. 7 shows the segmented CH scintillator analyzer (AT1-AT6);
- two neutron beam monitors located after the collimator are not shown [50].

Several different materials were tested as polarimeter targets (Table 1), to measure and compare their analyzing powers. These analyzers included C, CH_2, Cu as well as a CH active target with six elements (AT1–AT6). The downstream face of the analyzer block was located 10 cm before DC1. The energy deposit in the hadron calorimeter was used to select high-energy particles from the elastic-like events of interest, for example $\boldsymbol{p} + CH_2 \rightarrow p + X$, thus reducing contamination from inelastic scattering which produces lower-energy final-state hadrons. In addition it gave position information, which could be correlated with drift-chamber tracks.

The proton polarimeter used S0 and S1 to provide a trigger signal; drift chambers DC0, DC1 and DC2; C, CH_2 and Cu targets; the hadron calorimeter; while the neutron polarimeter used S3 and S4 to provide a trigger; drift chambers DC1 and DC2; CH, CH_2 and Cu targets; the hadron calorimeter. Where the active CH-scintillator analyzer was employed, it was also included in the trigger system. Further details on each component of the set-up are given below.

Table 1 Target material, density and length

Target	CH_2	CH	C	Cu
Density [g/cm^3]	0.919	1.06	1.68	8.96
Length [cm]	30	30	20	4

The scintillation counters were used to generate the trigger for the readout of data from all detectors in the set-up. Coincident hits from S0 (dimensions 200 × 200 × 10 cm) and S1 (dimensions 73 × 73 × 5 mm) were used to trigger on incident protons, during proton polarimetry measurements, whereas S3 and S4 (dimensions 240 × 240 × 20 mm), located downstream from the target were used in coincidence for triggering during neutron polarimetry measurements.

The drift chambers were used to reconstruct primary and secondary charged particle tracks and are described in detail in Ref. [51]. Here we summarize their properties. All chambers contain an (Ar_2CH_4) gas mixture and have alternating, orthogonal X and Y coordinate planes. DC0, of dimensions 12.5 × 12.5 cm, was located upstream from the target and has 8 planes (4X, 4Y). DC1 and DC2 have dimensions 25 × 25 cm and were located downstream of the target. DC1 has 8 planes (4X,4Y) while DC2 has 4 planes (2X,2Y). Corrections for misalignments were performed prior to track reconstructions. To reconstruct a track, hits in at least three chamber planes were required. The hit-position uncertainty provided by the chambers was < 100 μm, which produced an angu-

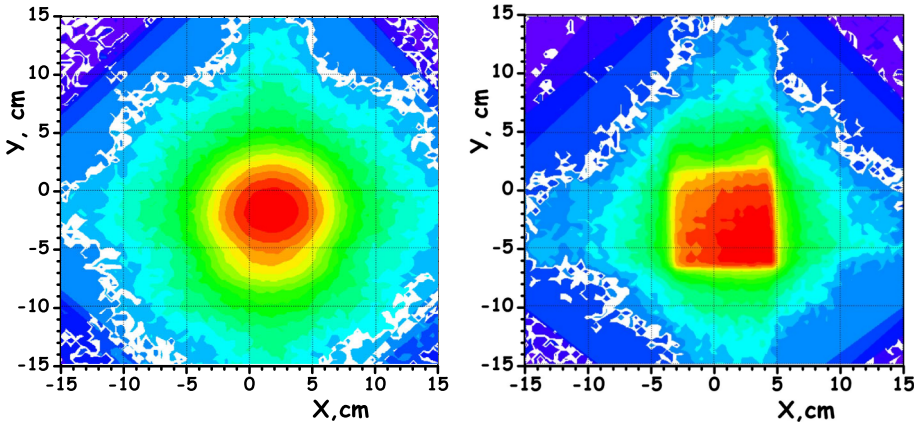

Fig. 8 Neutron (left) and proton (right) beam profiles in the transverse X–Y plane, as recorded by the drift chambers, for 3.75 GeV/c momentum and before a 30 cm long CH_2 target

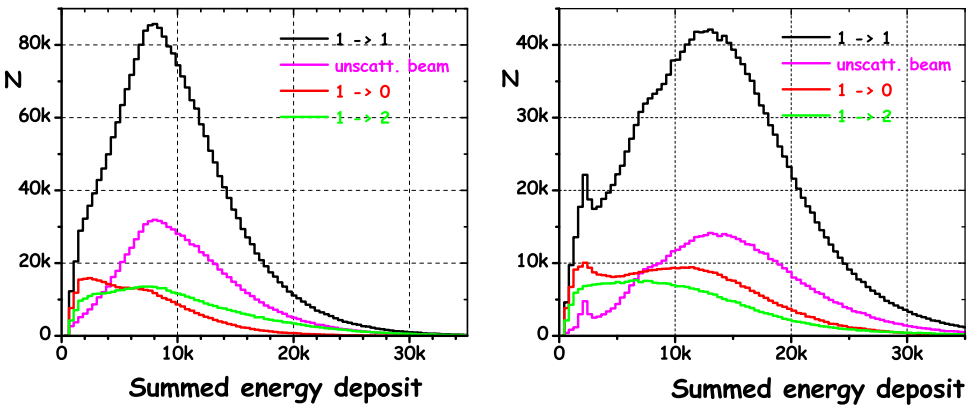

Fig. 9 Summed calorimeter energy deposit for different processes induced on a CH_2 target by protons of momentum 3.75 GeV/c (left) and 6.0 GeV/c (right)

lar resolution better than 0.4 mrad, and the reconstruction efficiency for charged tracks was close to 100%.

With proton beams, primary and scattered charged particle tracks were reconstructed using all drift chambers, while for neutron measurements primary signals were absent in DC0. Both protons and neutrons, incident on a nucleus, can produce multiple, charged, final-state particles and indeed some of the registered events have two or more hits in DC1 and DC2. A "clean" neutron charge exchange produces one energetic forward proton.

Examples of the proton and neutron beam profiles, as reconstructed by the chambers are shown in Fig. 8. The profile is given by the drift chambers that detect directly the proton beam, while, in the case of neutron beam, drift chambers detect charged particles generated from the interaction of the neutron beam in the target.

The hadron calorimeter, located at the downstream end of the polarimeter increased the fraction of useful, elastic-like events selected. Examples of the hadron calorimeter response, from protons incident on a CH_2 target, are given in Fig. 9. The response has been sorted into four categories: no interaction with the target (NI); no final-state charged particle ($1 \rightarrow 0$); one final-state charged particle ($1 \rightarrow 1$); two final-state charged particles ($1 \rightarrow 2$). The $1 \rightarrow 1$ category is the selected one to obtain the analyzing power.

It is separated from the NI category on the basis of the angle between incoming and outgoing tracks, which is chosen to be $> 1.7°$ to exclude multiple Coulomb scattering.

In the case of a neutron beam making a charge exchange in the target, the events of interest are no incident charged and one final-state charged particle ($0 \rightarrow 1$).

When the proton beam momentum increases from 3.75 GeV/c to 6 GeV/c, the proportion of $1 \rightarrow 1$ events decreases dramatically. Other processes, such as NI or $1 \rightarrow 2$, are enhanced relative to $1 \rightarrow 1$ which decreases the scattering asymmetry if they are not excluded. Neutron induced reactions are expected to have a similar behavior when the beam momentum increases. Placing a threshold on the summed energy deposit of the hadron calorimeter helps to identify the useful reactions. This is shown in Fig. 9, where the number of events corresponding to each type is shown as a function of the sum of the energy deposited in the calorimeter, at 3.75 GeV/c (left) and 6.0 GeV/c (right) for a CH_2 target. The ability of the hadron calorimeter to select high-energy nucleons will be extremely important to the forthcoming JLab EMFF experiments [18,20], which will operate at very high luminosity, where the electron beam will generate a huge flux of low-momentum background. The hadron calorimeter will provide the primary trigger for the nucleon arm of these experiments and the selection of high momen-

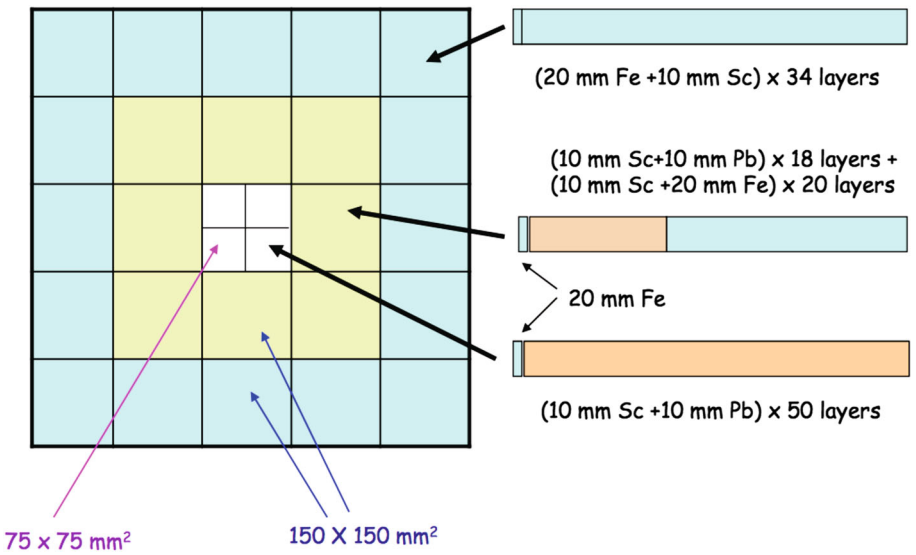

Fig. 10 View of the different bars of the hadron calorimeter used in the ALPOM2 set-up. The different bar compositions are noted at the side

tum particles through their energy deposit will be vital for suppressing soft background in the polarimeter. Furthermore it will help to select nucleons produced at forward angles where the analyzing power will be largest.

The hadron calorimeter, built in Dubna for the COMPASS experiment at CERN [52,53], is a sampling calorimeter composed of alternating plates of plastic-scintillator and iron or lead. The iron/lead provides most of the stopping power for energetic hadrons, so that the incident energy is totally absorbed in a thickness less than 1 m. As used in ALPOM2, it comprises 28 elements (Fig. 10). Four bars with dimensions 75×75 mm, were used in the central region, at smaller scattering angles, where higher count rates were experienced, whereas at larger scattering angles, 24 bars with dimensions of 150×150 mm were used.

As shown in Fig. 10, different bars have different arrangements of iron (Fe), lead (Pb) and scintillator (Sc) that was 10 mm thicker in comparison with the original COMPASS bar. The azimuthal angle selection, determined by the segmentation of the calorimeter and subsequently used in presentations of asymmetries, is given in Fig. 11.

The response of all calorimeter bars and their associated electronics was calibrated in dedicated cosmic-ray runs, where the hadron calorimeter was rotated by 90° so that the bars were aligned vertically. Further calibrations, with the calorimeter in standard alignment, were performed with the proton beam. The results are shown in Table 2 and in Fig. 12.

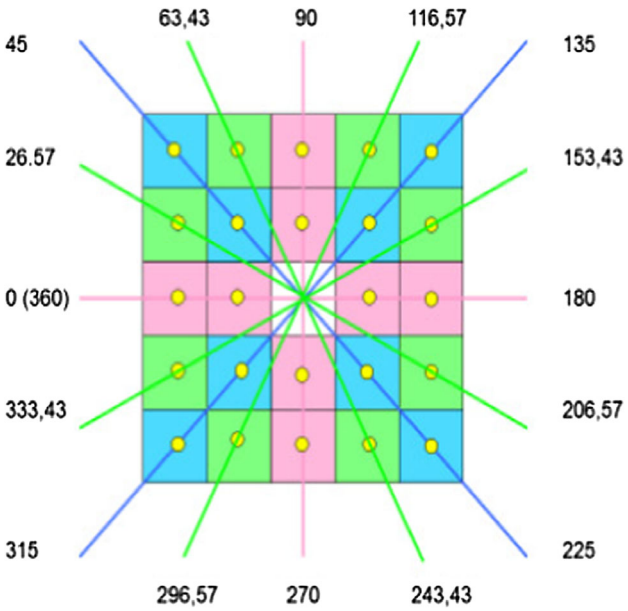

Fig. 11 Azimuthal angles corresponding to the central points of the hadron calorimeter bars

2.4 Readout and data acquisition

Signals from the detectors were first shaped and processed by a combination of custom made front-end electronics, and subsequently readout via a VMEbus data acquisition (DAQ) system. The DAQ controlled data readout from several VMEbus modules, including a trigger control module, a multi-hit scaler, multi-hit time-to-digital converters (TDCs), and time and charge waveform sampling digitizers (TQDCs). The DAQ electronics, online software and modules were developed by the AFI electronic group of JINR [51].

The TDCs were used to record signal times from the drift chambers, scintillation counters and a flag giving the polarisation state of the deuteron beam, whereas, the TQDCs were used to record signal timing and amplitude from the hadron calorimeter and active CH analyzer. A time resolution of 100 ps was provided by the TDC and TQDC modules.

Table 2 The peak energy deposit (channel) and the peak width (FWHM) are given for a proton beam on a CH_2 target and for a neutron beam on an active target (CH), after the hadron calorimeter calibration with cosmic rays

Particle [GeV/c]	Momentum [GeV]	T	Energy [channel]	Width [channel]
Proton	3.00	2.205	7300	3400
Proton	4.20	3.365	11100	4700
Proton	3.75	2.927	10,000	4500
Neutron	3.75	2.926	9700	4600

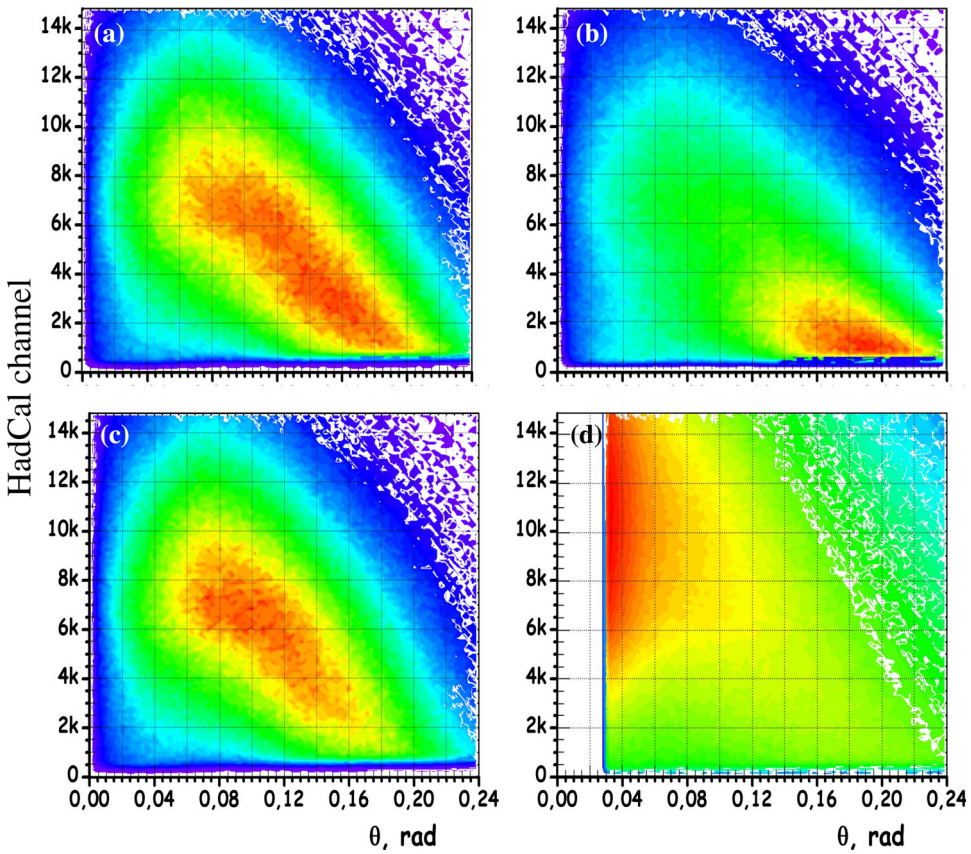

Fig. 12 Hadron calorimeter summed energy deposit vs. particle angle for (**a**) $n + C$, (**b**) $n + Cu$, (**c**) $n + CH_2$, and (**d**) $p + CH_2$. In subfigure (**d**) the events corresponding to the unscattered beam are removed by a small-angle cut

3 Data analysis and results

In Fig. 13, the left–right asymmetries from the F3 polarimeter for each state of beam polarization are displayed as a function of the run number, together with lines denoting the mean values. This demonstrates the excellent stability of the beam polarization throughout the data taking, as well as a small difference between the asymmetries obtained in the different polarization modes.

The results on analyzing powers given here are based on the following values of the nucleon polarization:

$(P^-, P^+) = (0.302, 0.590)$ for the runs in November 2016 and $(P^-, P^+) = (0.434, 0.525)$ for the runs in February 2017, to which we attribute an error $\leq 10\%$.

The analysis procedure is described as follows. Incoming and outgoing trajectories were reconstructed from the drift chambers, the azimuthal and polar angles calculated and their histograms built for each polarization state of the beam. The results are plotted as functions of the transverse momentum $p_t = p_{lab} \sin\theta$, which may be related approximately to the Mandelstam variable t, by $p_t \simeq \sqrt{-t}$. The considered process not being completely elastic, the variable t is not directly related to the momentum transferred to the system.

3.1 Nucleon yield distributions

The nucleon yield distributions as a function of p_t^2 are displayed in Fig. 15, for $p + CH_2$ scattering and in Fig. 14, for $n + C$ scattering at momentum 3.75 GeV/c. The analysis has been limited to the kinematic region $p_t < 0.4$ GeV/c in order to avoid the very large corrections where the acceptance of the polarimeter is low. These distributions are the convo-

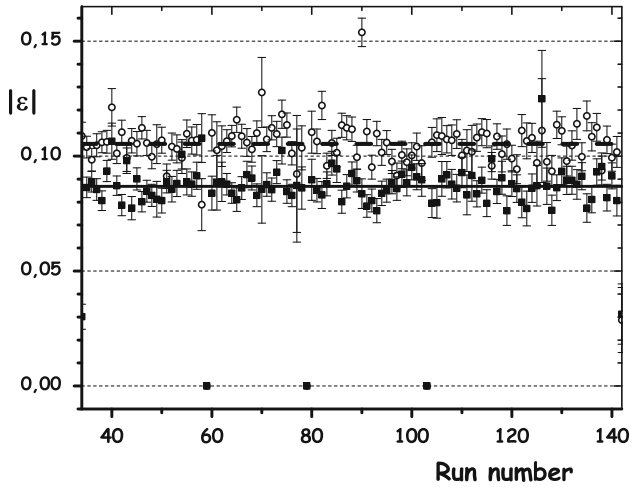

Fig. 13 Left–right asymmetry, ϵ (modulus) from F3, for each polarization state as a function of the run number during the data taking

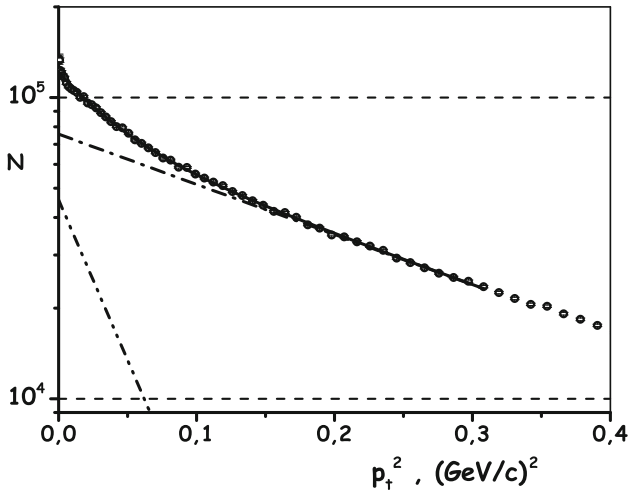

Fig. 14 p_t^2-distribution for $n+C$ scattering events at 3.75 GeV/c (arbitrary units). The solid line is the sum of exponential functions, the dot-dot-dashed and the dot-dashed lines correspond, respectively, to the two contributions with slope parameters b_1 and b_2

lution of physical processes and finite resolution effects of the detection system. The differential cross section for elastic nucleon scattering in the GeV region is in general well described by a sum of t-dependent exponentials:

$$\frac{d\sigma}{dt} = \sum_i c_i \exp(b_i t).$$

Thus, in the p_t^2 representation, a satisfactory description of the data in terms of a similar exponential sum is expected:

$$\frac{d\sigma}{dp_t^2} = \sum_i c_i \exp(-b_i p_t^2),$$

where the parameters b_i and c_i were determined from fits to the distributions of Fig. 14 with the help of the software package FUMILI [54].

Early studies of np elastic scattering have been made at energies below 6 GeV [48,55] and in the range 5–30 GeV [56]. They show that np cross sections are similar to pp cross section, with similar slopes, which implies that the interaction radii are similar. The np system shows a shrinkage of the diffraction peak with increasing energy.

The p_t-distribution for $n + C$ scattering at 3.75 GeV/c is presented in Fig. 14. The distribution is described by the sum of two exponential functions with slope parameters $b_1 = 24.5$ (GeV/c)$^{-2}$ and $b_2 = 3.2$ (GeV/c)$^{-2}$. To our knowledge there are no previous data to compare with the present $n + C$ slopes.

The p_t^2 distribution for $p + CH_2$ scattering at 3.75 GeV/c is described by the sum of three exponential functions. The first, whose form is related to multiple, small-angle Coulomb scattering convoluted with the experimental angular resolution, is not shown in Fig. 15. The slope parameter for the second function is $b_2' = 71.3 \pm 0.2$ (GeV/c)$^{-2}$, which is

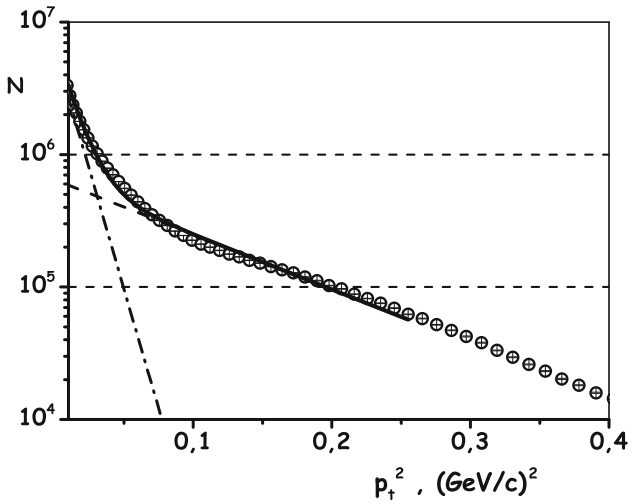

Fig. 15 p_t^2-distribution for $p + CH_2$ scattering events at 3.75 GeV/c (arbitrary units). The solid line is the sum of exponential functions, the long dashed and the dot-dashed lines correspond to the two contributions with slope parameters b_2' and b_3', respectively

close to the slope parameter for $p + C$ elastic scattering, previously determined to be 69 ± 4 (GeV/c)$^{-2}$ [57]. The third component has $b_3' = 7.4 \pm 0.1$ (GeV/c)$^{-2}$, which is close to the slope of pp elastic scattering, which varies between 7 and 8.

3.2 Analyzing powers

The number of events detected in a unit solid angle around the direction of the scattered particle, for beam-polarization states "+" and "−", $N^{\pm}(\theta, \phi)$, is

$$N^{\pm}(\theta, \phi) = N_0^{\pm}(\theta)(1 \pm P^{\pm} A_y(\theta) \cos\phi). \quad (2)$$

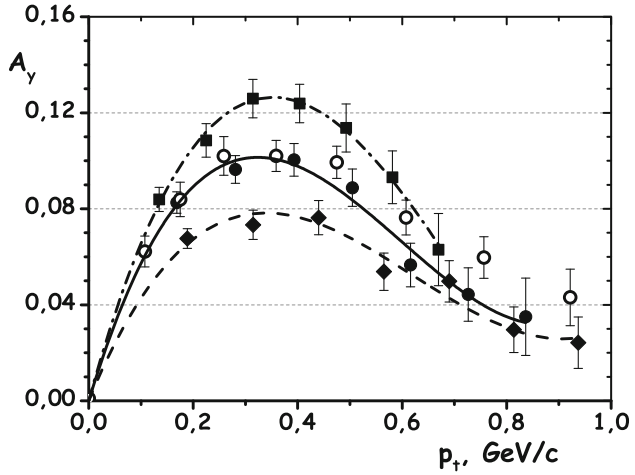

Fig. 16 A_y for $p+CH_2 \rightarrow$ one charged particle $+X$ at beam momenta 3.0 GeV/c (solid squares), 3.75 GeV/c (solid circles), and 4.2 GeV/c (solid diamonds) measured in this experiment, compared to previous data from Ref. [2] at beam momentum 3.8 GeV/c (open circles). The lines represent guides to the eye through the data points

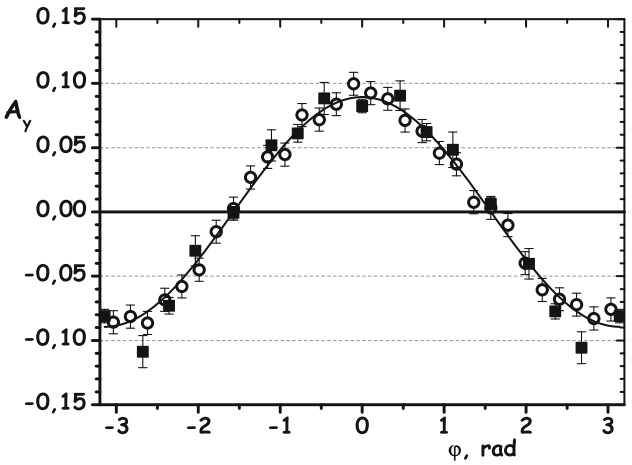

Fig. 17 A_y for $p + CH_2$ scattering at a momentum 3.0 GeV/c determined from the hadron calorimeter (filled black squares), compared to averaged values determined from the tracks (empty circles)

The beam polarization did not have the same value in the two states, *i.e.*, $P^+ \neq P^-$. $N_0^{\pm}$ is the number of events for unpolarized beam, where the superscript $\pm$ indicates that the beam intensity was different in the two polarization states, requiring a different normalization, $\alpha = N_0^-/N_0^+$. Instead of θ, the variable p_t is preferred. The analyzing power and its error are derived for each p_t beam, from a linear fit in $\cos\phi$ using the following formula:

$$A_y(p_t)\cos\phi = \frac{N^+(p_t,\phi) - \alpha N^-(p_t,\phi)}{N^+(p_t,\phi)P^- + \alpha N^-(p_t,\phi)P^+}. \qquad (3)$$

In this way we also cancel experimental asymmetries, due, for example, to apparatus or beam misalignment, which are present for all beam-polarization states. The related statistical error is derived by propagating the errors on $N^{\pm}$ and $P^{\pm}$.

The main source of systematic error on the analyzing power comes from the precision with which the beam polarization is known.

The present analyzing powers for $p + CH_2$ at 3.0 GeV/c (solid squares) 3.75 GeV/c (solid circles), and 4.2 GeV/c momenta (solid diamonds in Fig. 16) are consistent with previous data obtained at 3.8 GeV/c (open circles) [2]. All displayed data follow a similar p_t- dependence and show a systematic decrease of A_y with increasing incident momentum.

The scattering asymmetry can be derived independently from the angle information given both by DC1, DC2 and by the hadron calorimeter. In order to check the reliability of the analysis based on drift chambers we also reconstructed the asymmetry from the hadron calorimeter, without the central four small bars, although with coarser granularity in the azimuthal angle. The results for $p+CH_2$ at 3.0 GeV/c momentum are shown in Fig. 17 (filled squares). They are compared to the DC1, DC2 analysis averaged over polar angles $0.03 \leq \theta \leq 0.24$ rad (empty circles). The averaging produces a maximum value of A_y that is slightly smaller than the corresponding maximum in Fig. 16.

A_y for the $n + CH_2$ charge-exchange reaction (one final-state, detection of one charged particle) is shown in Fig. 18 (top) at different momenta and in Fig. 18 (bottom) for different polarimeter targets. A_y appears to decrease slightly with increasing neutron momentum, but the effect is much weaker than in $p + CH_2$ scattering. The dependence of A_y on target material is very weak and there is no significant difference between data on C, CH, CH_2 and Cu.

Compared to the previous results from Refs [39,40], obtained on charge-exchange reactions on a free polarized proton target, the measured analyzing powers of Fig. 18 are smaller, due to contamination of the signal by inelastic processes. Partial suppression on inelastic contamination is studied below. Moreover, the observable previously measured, called 'Pol' in those papers, has opposite sign. The experimental situation was essentially different, and the notations are those commonly used for elastic scattering: the neutron beam was incident on a polarized proton target, and the recoil proton was measured. The sign of the polarization vector was fixed with respect to the vector product of the incident and outgoing neutrons. In our case the neutron beam is polarized, and we detect the recoil charge particle. Our reference axis is the vector product of incident neutron and detected charge particle that is therefore opposite in c.m.s.

Charge exchange can also be studied for the process $p + CH_2 \rightarrow n + X$, where neutral particles are detected with the condition that no charged track is recorded in DC1, DC2, but there is a suitably high-energy deposit in the hadron calorimeter, from the interaction of a forward neutron.

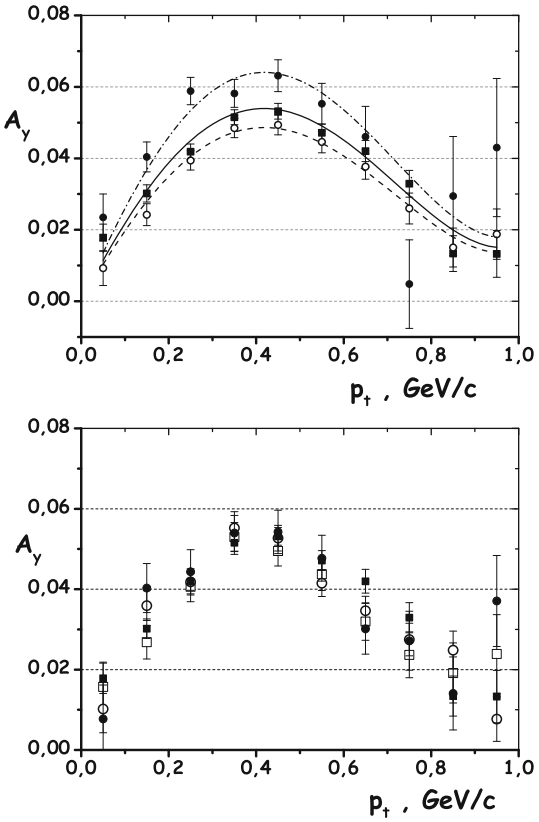

Fig. 18 A_y as a function of p_t: (top) for $n + CH_2$ scattering at neutron different momenta: 3 GeV/c (solid circles), 3.75 GeV/c (solid squares), 4.2 GeV/c (open circles)- the lines represent eye guides through the data points; (bottom) for 3.75 GeV/c incident neutrons on different polarimeter targets: on CH_2 (solid squares), CH (open circles), C (open squares), and Cu (solid circles)

The values of A_y are similar to those obtained with a neutron beam and, contrary to the $p + CH_2 \rightarrow p + X$ scattering case, there is little appreciable dependence of A_y on the incident momentum.

For the first time, data were taken with 3.75 GeV/c polarized protons and neutrons incident on a Cu target, detecting a forward-emitted charged particle. Figure 19 compares A_y for charge-exchange $n + Cu \rightarrow p + X$ with the one for quasi-elastic $p + Cu \rightarrow p + X$. Where no threshold has been placed on the energy deposit from the hadron calorimeter, A_y for $p + Cu$ is roughly double that for $n + Cu$. However, after selection of events with hadron calorimeter energy deposit greater than 6000 [channels], A_y for $n + Cu$ increases by a factor ~ 2, while the increase for $p + Cu$ is ~ 1.3. This leads to an increase of the figure of merit for the $n + Cu$ charge-exchange reaction of almost 40%. Before selection, the figure of merit for neutron scattering on a 4 cm thick Cu target was evaluated as $8.0 \cdot 10^{-5}$, and after selection it increased up to $1.1 \cdot 10^{-4}$. The systematic errors of those values are in the range from - 10 to + 20%, due to the uncertainty in the estimation of the trigger efficiency and of the angular acceptance of the setup.

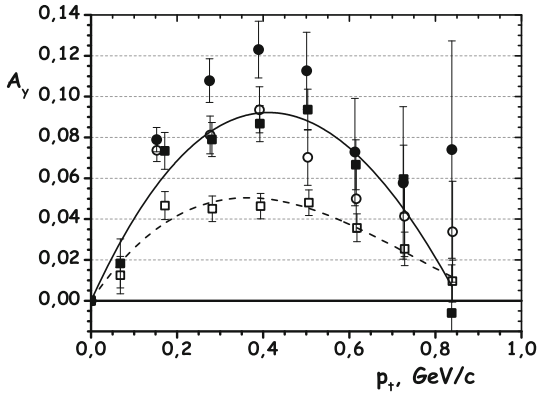

Fig. 19 p_t-dependence of A_y for quasi-elastic $p + Cu \rightarrow$ one charged particle $+X$ as open circles (solid circles) and charge-exchange $n + Cu \rightarrow$ one charged particle $+X$ as open squares (solid squares), for incident p and n momentum of 3.75 GeV/c before (after) selection of events with large energy deposit ($>$ 6000 [channels]) in the calorimeter. The lines represent eye guides through the data points for $n + Cu \rightarrow p + X$ before selection (dashed line) and after selection (solid line)

4 Conclusions

Analyzing powers for polarized protons and neutrons scattering on C, CH, CH_2 and Cu targets were measured at nucleon momenta from 3.0 to 4.2 GeV/c with the ALPOM2 polarimeter at JINR Dubna. The unique polarized deuteron beam from the Nuclotron accelerator, which has a maximum momentum of 13 GeV/c, has been used to produce both polarized protons and (for the first time) polarized neutrons.

Analyzing powers have been obtained for elastic-like proton scattering and charge-exchange neutron scattering, both of which entail detection of a single, forward charged particle. Selection of high-energy particles, using energy deposit in the calorimeter, is found to boost the analyzing power by a factor ~ 2 in the neutron case and ~ 1.3 in the proton case. Analyzing powers have also been obtained for charge-exchange proton scattering, yielding values which are very similar to the neutron charge-exchange case. The measured analyzer materials include C, CH, CH_2, and Cu, and show that A_y in the multi-GeV/c domain is essentially the same for light and heavy nuclei. A heavy nucleus analyzer has the advantage of being much more compact for a given effective thickness of material.

Two polarimeter features, namely: the implementation of a calorimeter for the selection of high-energy, final-state nucleons, and the replacement of a hydrogen-rich light target by heavier nuclei, open the way to simpler and more effective polarization measurements for proton and neutrons in the GeV region. Future experiments at JLab, requiring recoil-nucleon polarimetry, have already integrated these concepts, as in the case of experiments E12-07-109 [18] and E12-17-004 [20].

These polarimetry concepts have also a range of applications at JINR. The inverse reaction $p + Cu$ (or W)$\rightarrow n + X$, with neutron detection in the forward direction by a hadron calorimeter, can be used for measurement of the proton polarization at the NICA collider. Spin effects in hadronic and heavy-ion collisions may be studied at NICA, using non-polarized, longitudinally and transversally polarized beams, constituting a consistent spin physics program [58].

Acknowledgements The authors are grateful to the JINR-VBLHEP directorate for supporting their experiment, and the Nuclotron accelerator team, in particular the polarized deuteron source for providing them with a stable and high quality beam. This work has been partially supported by Université Paris-Saclay under grant P2I-ALPOM, by the Slovak Grant Agency VEGA under grant No. 1/0113/18, and by the UK Science and Technology Facilities Council under grants No. 57071/1 and No. 50727/1.

Data Availability Statement This manuscript has no associated data or the data will not be deposited. Authors' comment: Data are illustrated in Figures. Numbers are available from the authors in tabulated form upon request.]

5 Appendix: calculation of the analyzing powers

The calculation of analyzing power is based on the analysis of the two (φ, p_t)-plots corresponding to the two different polarization modes. We denote the bin values as $N_{ij}(1)$, $N_{ij}(2)$, where the first index, i, is related to φ and the second one, j, is related to p_t.

The values of the vector analyzing power b_j are obtained from a fit that minimizes the following quantity:

$$\sum_{i,j}\left(\frac{R_{ij} - b_j f(\varphi)_i}{\Delta R_{ij}}\right)^2, \tag{4}$$

with

$$R_{ij} = \frac{N_{ij}(2) - C \cdot N_{ij}(1)}{C \cdot N_{ij}(1)P(2) + N_{ij}(2)P(1)}, \tag{5}$$

$$\Delta R_{ij} = \sqrt{\frac{N_{ij}(1)N_{ij}(2)}{[N_{ij}(1) + N_{ij}(2)]^3}} \cdot \frac{2}{|P(2) + P(1)|}, \tag{6}$$

where $P(k)$ refers to the beam polarization, $k = 1, 2$ relates to the polarization mode, and

$$C = \frac{I[P(2)]}{I[P(1)]}$$

is the ratio of intensities (I) in the different polarization modes.

The fit is not equivalent to a number of j independent fits:

$$\sum_{i}\left(\frac{R_{ij} - b_j f(\varphi)_i}{\Delta R_{ij}}\right)^2 = min, \tag{7}$$

because the parameter C is common for all j and can be taken as a free parameter. Such a fit provides reliable results due to the small correlation existing between C and b_j in Eqs. (4) and (5) ($< 0.5\%$).

This program is included into the latest FUMILIM package, Ref. [59].

References

1. N.E. Cheung et al., Calibration of the polarimeter POMME at proton energies between 1.05 and 2.4-GeV. Nucl. Instrum. Meth. **A363**, 561–567 (1995)
2. L.S. Azhgirey, V.A. Arefev, S.N. Basilev, YuP Bushuev, V.V. Glagolev et al., Measurement of analyzing powers for the reaction $\boldsymbol{p} + CH_2$ at p_p = 1.75-GeV/c - 5.3-GeV/c. Nucl. Instrum. Meth. **A538**, 431–441 (2005)
3. F. Lehar, Current experiments using polarized beams of the JINR LHE accelerator complex. Phys. Part. Nucl. **36**, 501–528 (2005). [Fiz. Elem. Chast. Atom. Yadra 36,955 (2005)]
4. V.P. Balandin et al., Measurement of analyzing power for the reaction $\boldsymbol{p}$ + CH_2 at polarized proton momentum of 7.5 GeV/c (ALPOM2 proposal). Phys. Part. Nucl. **45**(1), 330–332 (2014)
5. V.D. Kekelidze, V.A. Matveev, I.N. Meshkov, A.S. Sorin, G.V. Trubnikov, Project nuclotron-based Ion collider facility at JINR. Phys. Part. Nucl. **48**(5), 727–741 (2017)
6. V.D. Kekelidze, NICA project at JINR: status and prospects. JINST **12**(06), C06012 (2017)
7. Simone Pacetti, Rinaldo Baldini Ferroli, Egle Tomasi-Gustafsson, Proton electromagnetic form factors: basic notions, present achievements and future perspectives. Phys. Rep. **550–551**, 1–103 (2015)
8. V. Punjabi, C.F. Perdrisat, M.K. Jones, E.J. Brash, C.E. Carlson, The structure of the nucleon: elastic electromagnetic form factors. Eur. Phys. J. A **51**, 79 (2015)
9. A.I. Akhiezer, M.P. Rekalo, Polarization phenomena in electron scattering by protons in the high energy region. Sov. Phys. Dokl. **13**, 572 (1968)
10. A.I. Akhiezer, M.P. Rekalo, Polarization effects in the scattering of leptons by hadrons. Sov. J. Part. Nucl. **4**, 277 (1974)
11. M.K. Jones et al., G_{Ep}/G_{Mp} ratio by polarization transfer in $\boldsymbol{e}p \rightarrow \boldsymbol{e}\boldsymbol{p}$. Phys. Rev. Lett. **84**, 1398–1402 (2000)
12. V. Punjabi, C.F. Perdrisat, K.A. Aniol, F.T. Baker, J. Berthot et al., Proton elastic form-factor ratios to Q^2 = 3.5 GeV^2 by polarization transfer. Phys. Rev. C **C71**, 055202 (2005)
13. O. Gayou et al., Measurement of G_{Ep}/G_{Mp} in $\boldsymbol{e}p \rightarrow \boldsymbol{e}\boldsymbol{p}$ to Q^2 = 5.6 GeV^2. Phys. Rev. Lett. **88**, 092301 (2002)
14. A.J.R. Puckett, E.J. Brash, O. Gayou, M.K. Jones, L. Pentchev et al., Final analysis of proton form factor ratio data at $q^2 = 4.0$, 4.8 and 5.6 gev^2. Phys. Rev. C **85**, 045203 (2012)
15. A.J.R. Puckett, E.J. Brash, M.K. Jones, W. Luo, M. Meziane et al., Recoil polarization measurements of the proton electromagnetic form factor ratio to Q^2 = 8.5 GeV^2. Phys. Rev. Lett. **104**, 242301 (2010)
16. A.J.R. Puckett et al., Polarization transfer observables in elastic electron proton scattering at $Q^2 = 2.5, 5.2, 6.8$, and 8.5 GeV^2. Phys. Rev. **C96**(5), 055203 (2017)
17. M. Meziane et al., Search for effects beyond the Born approximation in polarization transfer observables in $\boldsymbol{e}p$ elastic scattering. Phys. Rev. Lett. **106**, 132501 (2011)
18. C.F. Perdrisat, L.P. Pentchev, et al. Large Acceptance Proton Form Factor. Ratio Measurements at 13 and 15 (GeV/c)^2. Using Recoil Polarization Method, Jefferson Lab Experiment E12-07-109, 2007
19. B.D. Anderson et al. The Neutron Electric Form Factor at Q^2 up to 7(GeV/c)^2 from the reaction $^2H(\boldsymbol{e}, \boldsymbol{e'n})$ via Recoil Polarimetry, Jefferson Lab Experiment E12-11-009, 2011

20. J.R.M. Annand et al. Measurement of the Ratio G_E^n/G_M^n by the Double-polarized $^2H(\boldsymbol{e}, e'\boldsymbol{n})$ Reaction, Jefferson Lab Experiment E12-17-004, 2017
21. G. Cates et al. Measurement of the Neutron Electromagnetic Form Factor Ratio G_E^n/G_M^n at High Q^2, Jefferson Lab Experiment PR12-09-016, 2009
22. J. Becker et al., Determination of the neutron electric form-factor from the reaction $^3He(e, e'n)$ at medium momentum transfer. Eur. Phys. J. A **6**, 329–344 (1999)
23. T. Eden et al., Electric form factor of the neutron from the $^2H(\boldsymbol{e}, e'\boldsymbol{n})^1H$ reaction at $Q^2 = 0.255$ (GeV/c)^2. Phys. Rev. C **50**(4), R1749–R1753 (1994)
24. D.I. Glazier, M. Seimetz, J.R.M. Annand, H. Arenhovel, M Ases Antelo et al., Measurement of the electric form-factor of the neutron at $Q^2 = 0.3$ (GeV/c)^2 to 0.8 (GeV/c)^2. Eur. Phys. J. **A24**, 101–109 (2005)
25. J. Golak, G. Ziemer, H. Kamada, H. Witala, Walter Gloeckle, Extraction of electromagnetic neutron form-factors through inclusive and exclusive polarized electron scattering on polarized ^3He target. Phys. Rev. C **63**, 034006 (2001)
26. C. Herberg, M. Ostrick, H.G. Andresen, J.R.M. Annand, K. Aulenbacher et al., Determination of the neutron electric form-factor in the $D(e, e'n)p$ reaction and the influence of nuclear binding. Eur. Phys. J. A **5**, 131–135 (1999)
27. M. Meyerhoff et al., First measurement of the electric form-factor of the neutron in the exclusive quasielastic scattering of polarized electrons from polarized ^3He. Phys. Lett. B **327**, 201–207 (1994)
28. M. Ostrick, C. Herberg, H.G. Andresen, J.R.M. Annand, K. Aulenbacher et al., Measurement of the neutron electric form factor G_{En} in the quasifree $^2H(\boldsymbol{e}, e'\boldsymbol{n})p$ reaction. Phys. Rev. Lett. **83**, 276–279 (1999)
29. I. Passchier et al., The Charge form-factor of the neutron from the reaction polarized $^2H(\boldsymbol{e}, e'n)p$. Nucl. Phys. A **663**, 421–424 (2000)
30. Craig D. Roberts, Anthony G. Williams, Dyson–Schwinger equations and their application to hadronic physics. Prog. Part. Nucl. Phys. **33**, 477–575 (1994)
31. B. Plaster et al., Measurements of the neutron electric to magnetic form-factor ratio G_{En}/G_{Mn} via the $^2H(\boldsymbol{e}, e'\boldsymbol{n})^1H$ reaction to $Q^2 = 1.45$ (GeV/c)^2. Phys. Rev. C **73**, 025205 (2006)
32. R. Madey et al., Measurements of G_{En}/G_{Mn} from the $^2H(\boldsymbol{e}, e'\boldsymbol{n})$ reaction to $Q^2 = 1.45$ (GeV/c)^2. Phys. Rev. Lett. **91**, 122002 (2003)
33. S. Riordan et al., Measurements of the electric form factor of the neutron up to $Q^2 = 3.4$ GeV^2 using the reaction $^3\boldsymbol{He}(\boldsymbol{e}, e'n)pp$. Phys. Rev. Lett. **105**, 262302 (2010)
34. R. Diebold, D.S. Ayres, S.L. Kramer, A.J. Pawlicki, A.B. Wicklund, Measurement of the proton–neutron elastic-scattering polarization from 2–6 GeV/c. Phys. Rev. Lett. **35**, 632–635 (1975)
35. S.L. Kramer, D.S. Ayres, Daniel H Cohen, R. Diebold, A .J. Pawlicki, A .B. Wicklund, Polarization parameter for nucleon–nucleon elastic scattering at 11.8-GeV/c. Phys. Rev. D **17**, 1709 (1978)
36. H. Spinka et al., Beam polarization at the ZGS. Nucl. Instrum. Meth. **211**, 239–261 (1983)
37. I.G. Alekseev et al., Measurement of the carbon analyzing power for the momenta range 1.35 GeV/c to 2.02 GeV/c. Nucl. Instrum. Meth. **A434**, 254–260 (1999)
38. V.P. Ladygin. Analyzing power of pp and np elastic scattering at momenta between 2000 and 6000 MeV/c and polarimetry at LHE. Technical Report E13-99-123, Joint Inst. Nucl. Res., Dubna, (1999)
39. M.A. Abolins, M.T. Lin, R.C. Ruchti, J.G. Horowitz, R.C. Kammerud, N.W. Reay et al., Measurement of the polarization parameter in np charge–exchange scattering from 2 to 12 GeV/c. Phys. Rev. Lett. **30**, 1183–1185 (1973)
40. P.R. Robrish et al., Backward np scattering with a polarized target. Phys. Lett. **31B**, 617–620 (1970)
41. A. Kirillov et al. Relativistic polarized neutrons at the Laboratory of High-Energy Physics, JINR. In *Particles and nuclei. In: Proceedings, 14th international conference, PANIC'96, Williamsburg, USA, May 22-28, 1996*, pages 749–751, (1996)
42. V.I. Sharov et al., Measurement of the np total cross section difference $\Delta\sigma_L(np)$ at 1.39-GeV, 1.69-GeV, 1.89-GeV and 1.99-GeV. Eur. Phys. J. C **37**, 79–90 (2004)
43. N.N. Agapov, V.V. Fimushkin, V.P. Vadeev, V.P. Derenchuk, A.S. Belov. IUCF polarized ion source CIPIOS for JINR accelerator nuclotron. In *Spin physics. Polarized electron sources and polarimeters. In: Proceedings, 16th international symposium, SPIN 2004, Trieste, Italy, October 10–16, 2004, and Workshop, PESP 2004, Mainz, Germany, October 7-9, 2004*, pages 774–775, (2004)
44. V. Fimushkin, A.D. Kovalenko, L.V. Kutuzova, YuV Prokofichev, B. Shutov, A.S. Belov, V.N. Zubets, A.V. Turbabin, Development of polarized ion source for the JINR accelerator complex. J. Phys. **679**(1), 012058 (2016)
45. A. Abraham, *The Principles of Nuclear Magnetism*, vol. 32 (Oxford University Press, Oxford, UK, 1961)
46. B. Kuehn, C.F. Perdrisat, E.A. Strokovsky, Correlations between polarization observables in inclusive deuteron breakup. Phys. Atom. Nucl. **58**, 1795–1800 (1995). [Yad. Fiz.58,1898(1995)]
47. P. Rukoyatkin, Relativistic polarized beams for experiments on the polarized proton target at the laboratory of high energies. Czech. J. Phys. **51**, A345–A350 (2001)
48. J. Bystricky. F. Lehar, *Nucleon Nucleon Scattering Data - Summary Tables*, 1981 edn. (Karlsruhe, Germany, Fiz, 1981), p. 222 (Physics Data, 11–2)
49. B. Bonin et al., Measurement of the inclusive pC analyzing power and cross-section in the 1 GeV region and calibration of the new polarimeter POMME. Nucl. Instrum. Meth. A **288**, 379 (1990)
50. F. Lehar et al., Measurement of the total cross-section difference $\Delta\sigma^- L$ in np transmission at 1.19-GeV, 2.49-GeV and 3.65-GeV. Z. Phys. C **71**, 65–74 (1996)
51. V.V. Glagolev et al., STRELA experimental setup for studying charge–exchange processes. Nucl. Exp. Tech. **56**, 387–397 (2013)
52. N.V. Vlasov et al., A calorimeter for detecting hadrons with energies of 10–100 GeV. Instrum. Exp. Tech. **49**(1), 41–55 (2006)
53. Ph Abbon, E. Albrecht, VYu. Alexakhin, Yu. Alexandrov, G.D. Alexeev, M.G. Alekseev, A. Amoroso, H. Angerer, V.A. Anosov, B. Badełek et al., The COMPASS experiment at CERN. Nucl. Instrum. Meth. A **577**(3), 455–518 (2007)
54. I.M. Sitnik, Development of the FUMILI minimization package. Comput. Phys. Commun. **185**, 599–603 (2014)
55. M.N. Kreisler et al. Neutron-proton elastic scattering from 1 to 6.3 GeV. Technical report, Stanford University, SLAC Report n. 66, (1966)
56. B.G. Gibbard, M.J. Longo, Lawrence W Jones, J .R. O' Fallon, M .N. Kreisler, M .L. Perl, Neutron-proton elastic scattering from 5 to 30 GeV/c. Nucl. Phys. B **30**, 77–115 (1971)
57. J. Jaros et al., Nucleus–nucleus total cross-sections for light nuclei at 1.55-GeV/c/Nucleon and 2.89-GeV/c/Nucleon. Phys. Rev. C **18**, 2273–2292 (1978)
58. I. Savin, A. Efremov, D. Peshekhonov, A. Kovalenko, O. Teryaev, O. Shevchenko, A. Nagajcev, A. Guskov, V. Kukhtin, N. Toplilin, Spin physics experiments at NICA-SPD with polarized proton and deuteron beams. Eur. Phys. J. A **52**(8), 215 (2016)
59. I.M. Sitnik, Development of the FUMILIM minimization package. Comput. Phys. Commun. **209**, 199 (2016)